

QCD Dirac spectrum and components of the gauge field

Arata Yamamoto

Department of Physics, Faculty of Science, Kyoto University, Kitashirakawa, Sakyo, Kyoto 606-8502, Japan

(Dated: February 12, 2019)

We analyze the relation between the Dirac spectrum and the gauge field in SU(3) lattice QCD. We focus on how components of the gauge field are related to the Dirac spectrum. First, we consider momentum components of the gauge field. It turns out that the broad region of momentum components is relevant for the low-lying Dirac spectrum and zero modes, i.e., topological charges. The connection with chiral random matrix theory is also discussed. Second, we consider an SU(2) subgroup component of the SU(3) gauge field. The SU(2) subgroup component behaves like the SU(2) gauge field in the low-lying Dirac spectrum.

PACS numbers: 11.15.Ha, 12.38.-t, 12.38.Aw, 12.38.Gc

I. INTRODUCTION

The eigenvalue spectrum of the Dirac operator is a fundamental quantity in QCD. It reflects important properties induced by the gauge field. In particular, zero modes of the Dirac operator have special roles on nonperturbative properties of QCD. The numbers of zero modes determine the topological charge Q of the background gauge field, as

$$n_+ - n_- = Q, \quad (1)$$

where n_+ and n_- are the numbers of zero modes with positive and negative chirality, respectively [1]. Also, the existence of zero modes is related to spontaneous chiral symmetry breaking, through the Banks-Casher relation,

$$\pi\rho(0) = \Sigma, \quad (2)$$

where $\rho(0)$ is the macroscopic spectral density of zero modes and Σ is the absolute value of the chiral condensate [2].

Moreover, interestingly, the low-lying Dirac spectrum shows the universal behavior of disordered systems. Such an universal behavior is successfully described by chiral random matrix theory [3–5]. The distribution of the low-lying Dirac spectrum depends only on the global symmetries of the system, and not on the details of the microscopic structure. Once the validity of chiral random matrix theory is guaranteed, chiral random matrix theory enables us to predict the low-lying eigenvalue distribution by a simple and universal function.

It is definitely important to clarify how the gauge field induces these properties of the Dirac spectrum. However, it is rather difficult. These properties are beyond the reach of perturbation theory. Although the Dirac equation is written in a simple form, the low-energy Dirac spectrum is not easily obtained because of the complicated dynamics of the gauge field. In chiral random matrix theory, the information about the dynamics of the gauge field is lost.

The aim of this paper is to investigate the relation between the Dirac spectrum and the gauge field in lattice QCD. We focus on two kinds of components of the gauge

field: momentum components and subgroup components. We decompose the gauge field into some components, and then calculate the Dirac spectrum from the decomposed components. From the change of the Dirac spectrum, we analyze how the components of the gauge field are related to the Dirac spectrum. Although such a decomposition is gauge dependent, we can intuitively understand the role of the gauge field from this analysis.

In this paper, we calculate the staggered Dirac spectrum in lattice QCD. The basics of the staggered Dirac spectrum and the details of the numerical simulations are shown in Sec. II. For the analysis of momentum components, we introduce a lattice framework of momentum cutoff in Sec. III. We discuss the resultant Dirac spectrum and the connection with chiral random matrix theory. For the analysis of subgroup components, we project the SU(3) gauge field onto an SU(2) subgroup component, as demonstrated in Sec. IV. Finally, Sec. V is devoted to the summary.

II. THE DIRAC SPECTRUM IN LATTICE QCD

A. Staggered Dirac operator

The Euclidean Dirac operator is defined as

$$D = \gamma_\mu \partial_\mu - ig\gamma_\mu A_\mu. \quad (3)$$

The j -th eigenmode of the Dirac operator is given by

$$D\psi_j = i\lambda_j\psi_j. \quad (4)$$

The chirality is defined as

$$\chi_j = \psi_j^\dagger \gamma_5 \psi_j. \quad (5)$$

In continuum QCD, the anti-commutation relation,

$$\{D, \gamma_5\} = 0, \quad (6)$$

is satisfied. Because the Dirac operator is anti-Hermitian, λ_j is zero or nonzero real. Nonzero eigenvalues are always paired as $\pm i\lambda_j$ and their chiralities are zero. On the other

hand, zero eigenvalues are unpaired, and their chiralities are +1 or -1.

The staggered Dirac operator is

$$D = \frac{1}{2} \sum_{\mu} \eta_{\mu}(x) [\bar{U}_{\mu}(x) \delta_{x+\hat{\mu},y} - \bar{U}_{\mu}^{\dagger}(x - \hat{\mu}) \delta_{x-\hat{\mu},y}], \quad (7)$$

where $\eta_{\mu}(x)$ is the standard staggered phase factor. For the standard (unimproved) staggered Dirac operator, $\bar{U}_{\mu}(x)$ is the SU(3) link variable $U_{\mu}(x)$. For the improved staggered Dirac operator, $\bar{U}_{\mu}(x)$ is a combination of the link variables.

The staggered fermion describes the four-flavor Dirac fermion in continuum limit. At finite lattice spacing, however, there is an $O(a^2)$ term which violates the flavor symmetry and Eq. (6). Due to the presence of this term, the staggered Dirac spectrum does not have exact zero eigenvalues, unlike the continuum Dirac spectrum. As a result, the unimproved staggered Dirac operator fails to reproduce nontrivial topological sectors [6–8]. This problem is approximately settled by improving the gauge and fermion actions [9–12].

B. Simulation details

We computed the low-lying eigenvalues of the staggered Dirac operator by SU(3) quenched lattice QCD simulations [6–12]. We used the improved gauge action and the improved staggered Dirac operator.

For the gauge action, we adopted the 1-loop improved Symanzik gauge action with tadpole improvement. The 1-loop improved Symanzik gauge action includes the plaquette term, the 1×2 rectangle term, and the $1 \times 1 \times 1$ “parallelogram” term [13]. The tadpole coefficient is defined as the fourth-root of the average plaquette value [14]. As listed in Table I, we generated two kinds of quenched gauge configurations. The physical volumes of two gauge configurations are approximately the same. The finer one, $a \simeq 0.08$ fm and $V = 16^4$, is used for the analysis of the eigenvalues and the chiralities. The coarser one, $a \simeq 0.16$ fm and $V = 8^4$, is used for the connection with chiral random matrix theory.

For the staggered Dirac operator, we adopted the FAT7 \times ASQ operator [15]. The FAT7 \times ASQ operator is constructed from the FAT7 link variable and the ASQ operator [16]. This improved operator strongly suppresses the flavor-symmetry breaking lattice artifact. The spatial boundary conditions are periodic, and the temporal

TABLE I: The parameters of quenched gauge configurations. The lattice coupling β , the corresponding lattice spacing a , the lattice volume V , and the configuration number N_{conf} are listed.

β	a (fm)	V (a^4)	V (fm^4)	N_{conf}
8.6	0.08	16^4	1.3^4	50
7.9	0.16	8^4	1.3^4	5000

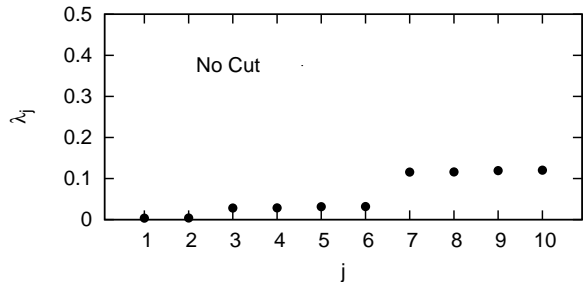


FIG. 1: The eigenvalue spectrum of the FAT7 \times ASQ Dirac operator. Only low-lying 10 positive eigenvalues of one typical gauge configuration are shown.

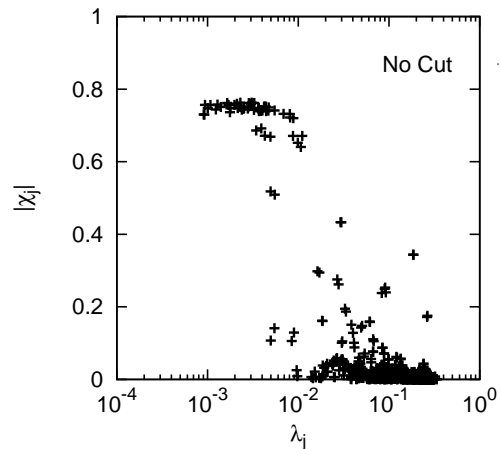


FIG. 2: The scattering plot of the eigenvalue λ_j and the absolute value of the chirality χ_j . The low-lying 30 eigenvalues of 50 gauge configurations are plotted. The calculation is done on 16^4 lattice with $\beta = 8.6$.

boundary condition is antiperiodic. Because the operator is anti-Hermitian, the eigenvalues always appear in pairs, $\pm i\lambda_j$. We only have to calculate the positive eigenvalues $\lambda_j > 0$. It should be understood that the negative eigenvalues with the same magnitude exist. We calculated the low-lying 30 positive eigenvalues.

In Fig. 1, we show the low-lying 10 positive eigenvalues of one typical gauge configuration of $\beta = 8.6$. The four-fold degeneracy, i.e., the four-flavor symmetry, is satisfied with high precision. In addition, zero eigenvalues are approximately reproduced. Such zero modes are called as “would-be” or “near” zero modes. Because the negative eigenvalues with the same magnitudes exist, the topological charge of this gauge configuration is $Q/N_f = 1$. In Fig. 2, we show the scattering plot of all the low-lying 30 eigenvalues of 50 gauge configurations of $\beta = 8.6$. There exists a clear separation between the nonzero modes, which is $|\chi_j| \simeq 0$, and the would-be zero modes, which is $|\chi_j| \simeq 0.8$. The reason why the chirality deviates from ± 1 is that it requires a renormalization [17].

III. ANALYSIS OF MOMENTUM COMPONENTS

In this section, we analyze how the Dirac spectrum is changed when the gauge field is restricted to some momentum components. Since the behavior of the gauge field depends on the energy scale, different momentum components would have different roles. In a different point of view, this analysis is connected with the relation between the energy scales of the fermion field and the gauge field.

A. Momentum cutoff

Here, we briefly introduce the lattice framework to remove some momentum components of the gauge field. For more details, see Refs. [18, 19]. The framework is formulated as the following five steps.

Step 1. The link variable $U_\mu(x)$ is generated by Monte Carlo simulation. The link variable is fixed with a certain gauge.

Step 2. The momentum-space link variable $\tilde{U}_\mu(p)$ is obtained by the Fourier transformation, as

$$\tilde{U}_\mu(p) = \frac{1}{V} \sum_x U_\mu(x) \exp(i \sum_\nu p_\nu x_\nu), \quad (8)$$

where V is the lattice volume.

Step 3. Some components of $\tilde{U}_\mu(p)$ are removed by introducing a momentum cutoff. In the cutoff region, the momentum-space link variable is replaced by the free-field link variable

$$\tilde{U}_\mu^{\text{free}}(p) = \frac{1}{V} \sum_x 1 \exp(i \sum_\nu p_\nu x_\nu) = \delta_{p0}. \quad (9)$$

For example, the ultraviolet cutoff Λ_{UV} is introduced as

$$\tilde{U}_\mu^\Lambda(p) = \begin{cases} \tilde{U}_\mu(p) & (\sqrt{p^2} \leq \Lambda_{\text{UV}}) \\ 0 & (\sqrt{p^2} > \Lambda_{\text{UV}}), \end{cases} \quad (10)$$

and the infrared cutoff Λ_{IR} is introduced as

$$\tilde{U}_\mu^\Lambda(p) = \begin{cases} \delta_{p0} & (\sqrt{p^2} < \Lambda_{\text{IR}}) \\ \tilde{U}_\mu(p) & (\sqrt{p^2} \geq \Lambda_{\text{IR}}). \end{cases} \quad (11)$$

Step 4. The coordinate-space link variable is obtained by the inverse Fourier transformation as

$$U'_\mu(x) = \sum_p \tilde{U}_\mu^\Lambda(p) \exp(-i \sum_\nu p_\nu x_\nu). \quad (12)$$

Since $U'_\mu(x)$ is not an $\text{SU}(3)$ matrix in general, $U'_\mu(x)$ must be projected onto an $\text{SU}(3)$ element $U_\mu^\Lambda(x)$. The projection is realized by maximizing the quantity

$$\text{ReTr}[\{U_\mu^\Lambda(x)\}^\dagger U'_\mu(x)]. \quad (13)$$

Step 5. The expectation value of an operator O is computed by using this link variable $U_\mu^\Lambda(x)$ instead of $U_\mu(x)$, i.e., $\langle O[U^\Lambda] \rangle$ instead of $\langle O[U] \rangle$.

Using this framework, we can analyze the relation between the physical quantity and momentum components of the gauge field. While the Dirac spectrum is gauge invariant, a momentum component of the gauge field is gauge variant. This is because a gauge transformation is nonlocal in momentum space. Thus, we must fix the gauge in Step 1. In this study, we calculated the eigenvalue spectrum of the Dirac operator $D[U^\Lambda]$ in the Landau gauge.

B. Eigenvalues and chiralities

We applied the above framework to the Dirac spectrum. In Fig. 3, we show the Dirac spectrum with $\Lambda_{\text{UV}} = 3 \text{ GeV}$ and $\Lambda_{\text{IR}} = 3 \text{ GeV}$. The original gauge configuration is the same as that of Fig. 1. For $\Lambda_{\text{UV}} = 3 \text{ GeV}$, while all the eigenvalues change, the four-fold degeneracy is still satisfied. The would-be zero modes which exist in Fig. 1 disappear. This means that the topological charge is broken. For $\Lambda_{\text{IR}} = 3 \text{ GeV}$, the low-lying 10 eigenvalues become close to the eigenvalue of free fermions, which is about 0.39 for this case. Also in this case, the topological charge becomes zero.

In Fig. 4, we show the scattering plot of the eigenvalue and the chirality with the ultraviolet cutoff Λ_{UV} . As the high-momentum component is removed, the eigenvalue spectrum is gradually changed. For $\Lambda_{\text{UV}} = 3 \text{ GeV}$, all eigenmodes are $|\chi_j| \simeq 0$. Therefore, all gauge configura-

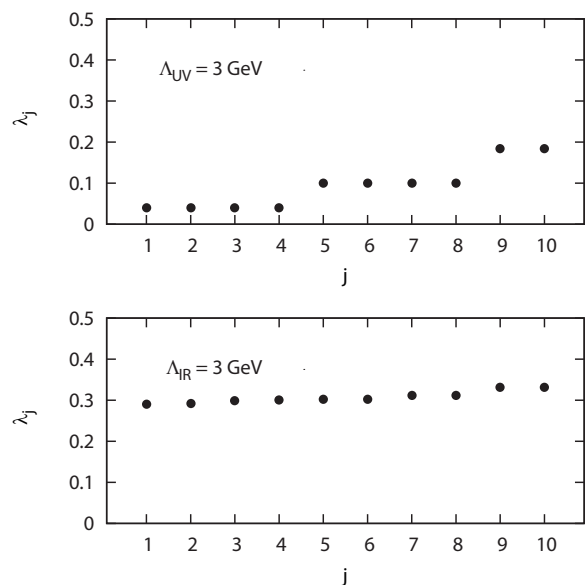


FIG. 3: The low-lying Dirac spectrum with the momentum cutoff. The original gauge configuration is the same as that of Fig. 1.

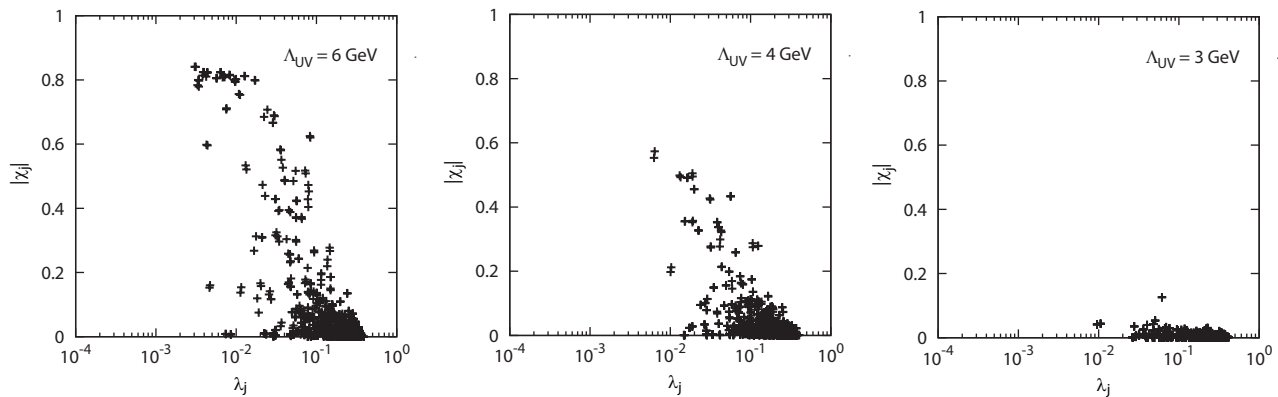


FIG. 4: The scattering plot of the eigenvalue λ_j and the absolute value of the chirality χ_j with the ultraviolet cutoff Λ_{UV} . The low-lying 30 eigenvalues of 50 gauge configurations with $\beta = 8.6$ are plotted.

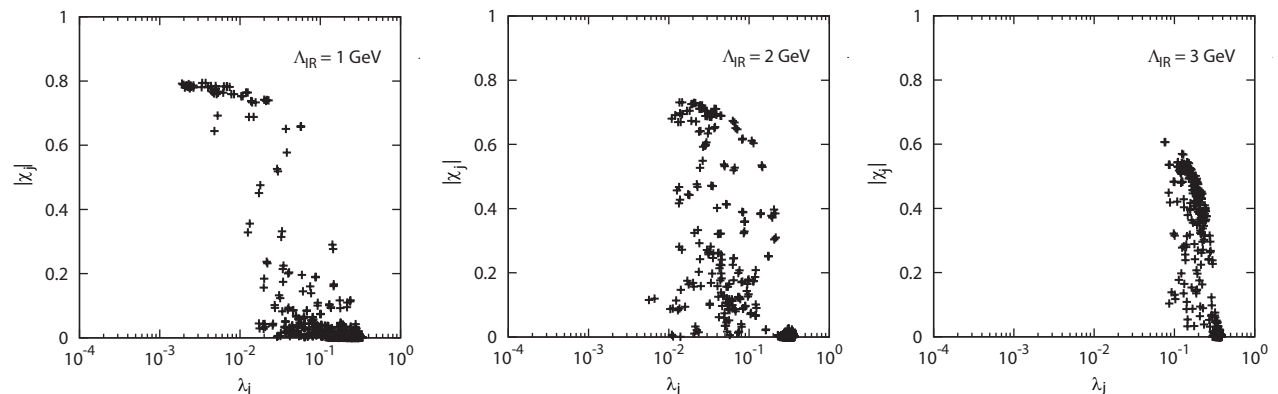


FIG. 5: The scattering plot of the eigenvalue λ_j and the absolute value of the chirality χ_j with the infrared cutoff Λ_{IR} . The low-lying 30 eigenvalues of 50 gauge configurations with $\beta = 8.6$ are plotted.

tions fall into the trivial topological sector.

The scattering plot with the infrared cutoff Λ_{IR} is shown in Fig. 5. When the low-momentum component is removed, many of the low-lying eigenvalues approach the free eigenvalue, which is $\lambda_j \simeq 0.39$ and $|\chi_j| \simeq 0$. Compared to the case of the ultraviolet cutoff, the changes of the eigenvalues are sensitive to the infrared cutoff. This result is consistent with our expectation that the low-lying Dirac eigenmode interacts with the low-momentum gauge field. For $\Lambda_{IR} = 3$ GeV, we cannot identify would-be zero modes since all eigenvalues are almost degenerate.

From these results, except for the very-high-momentum components, the relatively broad region of momentum components of the gauge field is related to the low-lying Dirac spectrum. In particular, zero modes are destroyed only after removing the broad region of momentum components. There seems to be no typical scale of the gauge field inducing zero modes, i.e., topological charges. This behavior is different from the behavior of confinement, which is induced only by the narrow low-momentum component of the gauge field [18–20].

When the momentum cutoff is imposed, the clear separation between would-be zero modes and nonzero modes

is lost. This is because the staggered Dirac operator does not have exact zero modes. This situation will be improved by the overlap operator, which has exact zero modes [21, 22].

C. Connection with chiral random matrix theory

Next, we compared the lattice data with a prediction of chiral random matrix theory, using the gauge configurations of $\beta = 7.9$. We analyzed the $Q = 0$ sector with the criterion for nonzero modes as $|\chi_j| < 0.1$.

We calculated the probability distribution of the lowest nonzero eigenvalue λ_{\min} . In chiral random matrix theory, the probability distribution of the lowest eigenvalue is given as

$$P(\lambda_{\min}) = \frac{z_{\min}}{2} e^{-z_{\min}^2/4} \quad (14)$$

$$z_{\min} \equiv \lambda_{\min} \Sigma V \quad (15)$$

for the SU(3) quenched gauge field with $Q = 0$ [23]. If one directly calculates the chiral condensate in infinite volume, this function is parameter free. In this study, we

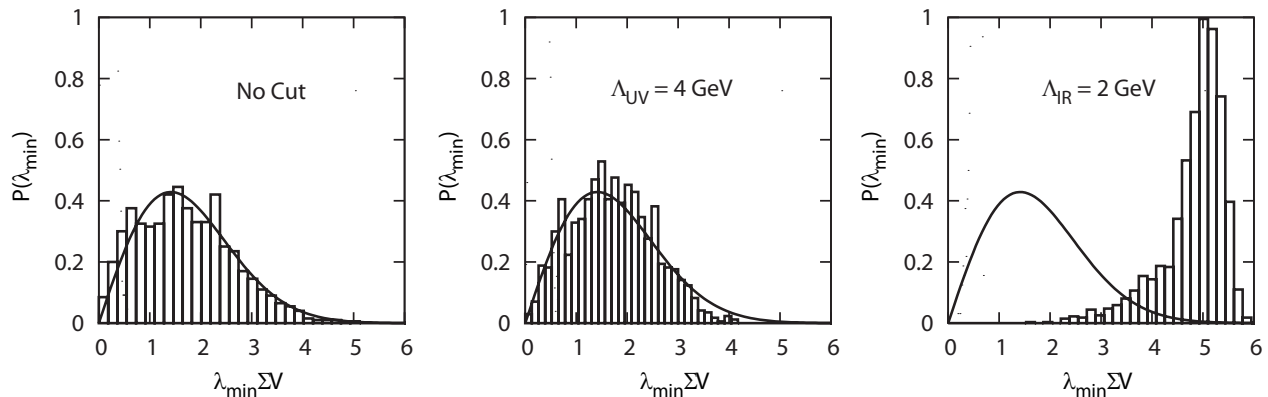


FIG. 6: The probability distribution of the lowest eigenvalue λ_{\min} in the $Q = 0$ sector. The histograms are the lattice data of 8^4 lattice with $\beta = 7.9$. The solid curves for No Cut and $\Lambda_{UV} = 4$ GeV are the best-fit functions of Eq. (14) from chiral random matrix theory.

treated Σ as a fitting parameter. The lattice data and the best-fit result of Eq. (14) are shown in Fig. 6. In the original lattice QCD (No Cut), the lattice data is well reproduced by chiral random matrix theory. The best-fit value is $\Sigma \simeq 0.0022 \times a^{-3}$.

For $\Lambda_{UV} = 4$ GeV, the qualitative behavior does not change. The lattice data is still reproduced by Eq. (14). Thus, the high-momentum component of the gauge field is irrelevant for the universality of the lowest eigenvalue distribution. The best-fit value of Σ is changed by the ultraviolet cutoff. This is because the chiral condensate is renormalization-group variant and ultraviolet divergent. By definition, the ultraviolet divergent quantity depends on the ultraviolet cutoff, although this might be irrelevant for phenomenology.

For $\Lambda_{IR} = 2$ GeV, the lowest eigenvalue distribution becomes to concentrate on the vicinity of the free eigenvalue. The lattice data drastically deviates from Eq. (14). Therefore, the low-momentum component of the gauge field is crucial for the validity of chiral random matrix theory. In other words, the low-momentum component induces the strong-interacting and disordered nature of the gauge field.

In a previous work, the chiral condensate was directly analyzed by the lattice framework of the momentum cutoff [24]. It suggests that the zero-momentum component of the gauge field has a large contribution to the chiral condensate. To check it in the present study, we calculated the Dirac spectrum with the small infrared cutoff $\Lambda_{IR} \sim 0.1$ GeV. For $\Lambda_{IR} \sim 0.1$ GeV, the lattice data can be fitted by Eq. (14) with the best-fit value $\Sigma \simeq 0.0019 \times a^{-3}$. The contribution of the zero-momentum component is indeed large, about 15% of the total. This is qualitatively consistent with the previous work. Note, however, that this is quantitatively different from the previous work because of many systematic differences.

IV. ANALYSIS OF SUBGROUP COMPONENTS

Although there are many similarities between the SU(2) and SU(3) gauge theories, there are several differences because of an additional symmetry of SU(2). An SU(3) group element includes SU(2) subgroup elements. In this section, we consider whether an SU(2) subgroup component of the SU(3) gauge field shows the same behavior as the SU(2) gauge field.

A. Subgroup projection

The framework of the subgroup projection is formulated as below.

Step 1. The link variable $U_\mu(x)$ is generated by Monte Carlo simulation. The link variable is fixed with a certain gauge.

Step 2. From the SU(3) link variable,

$$U_\mu(x) = \begin{pmatrix} U_{11} & U_{12} & U_{13} \\ U_{21} & U_{22} & U_{23} \\ U_{31} & U_{32} & U_{33} \end{pmatrix}, \quad (16)$$

the SU(2)-projected link variable is generated from its subgroup element, as

$$u_\mu(x) = \begin{pmatrix} U_{11} & U_{12} & 0 \\ U_{21} & U_{22} & 0 \\ 0 & 0 & 1 \end{pmatrix}. \quad (17)$$

Step 3. The expectation value of an operator O is computed by using this link variable $u_\mu(x)$ instead of $U_\mu(x)$, i.e., $\langle O[u] \rangle$ instead of $\langle O[U] \rangle$.

Also for the subgroup projection, we use the Landau gauge.

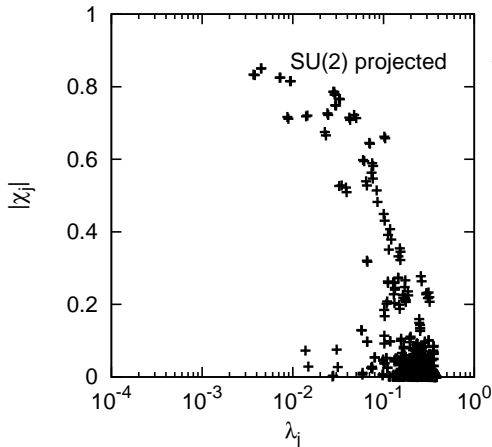


FIG. 7: The scattering plot of the eigenvalue λ_j and the absolute value of the chirality χ_j of the SU(2)-projected gauge field. The low-lying 20 eigenvalues of 50 gauge configurations with $\beta = 8.6$ are plotted.

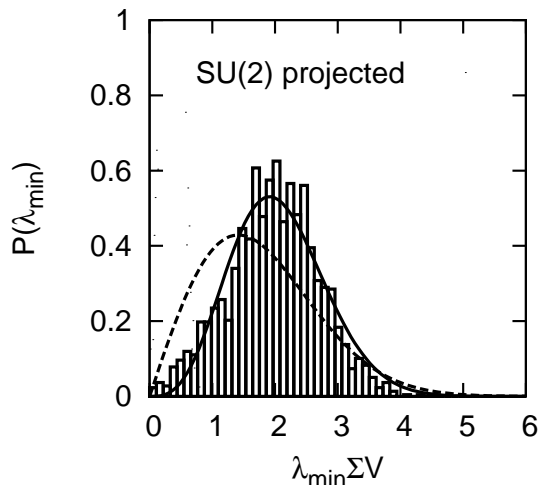


FIG. 8: The lowest eigenvalue distribution of the SU(2)-projected gauge field in the $Q = 0$ sector. The solid and dashed curves are Eqs. (18) and (14), respectively.

B. Numerical results

As shown in Fig. 7, the Dirac spectrum of the SU(2)-projected gauge field has would-be zero modes. Although the number of would-be zero modes changes, the qualitative behavior is similar to that of the original SU(3)

gauge field.

The low-lying Dirac spectrum depends on the symmetry of the fermion field [25]. For the staggered Dirac operator with the SU(2) quenched gauge field, chiral random matrix theory predicts that the lowest eigenvalue distribution is

$$P(\lambda_{\min}) = (z_{\min} \cosh z_{\min} - \sinh z_{\min}) e^{-z_{\min}^2/2} \quad (18)$$

in the $Q = 0$ sector [23]. This distribution is observed in SU(2) lattice QCD [26]. In Fig. 8, we show the lattice data of the SU(2)-projected gauge field. The solid and dashed curves are the predictions of chiral random matrix theory for SU(2) and SU(3), i.e., Eqs. (18) and (14), respectively. The lattice data is reproduced by the prediction for SU(2), not for SU(3). Therefore, the SU(2) subgroup component of the SU(3) gauge theory shows the same universal behavior as the SU(2) gauge theory.

V. SUMMARY

We investigated the relation between Dirac spectrum and components of the gauge field in the Landau gauge. We considered momentum components and a subgroup component of the gauge group. For momentum components of the gauge field, the broad region of the momentum components is relevant for the low-lying Dirac eigenvalues. The low-momentum component is crucial for the validity of chiral random matrix theory. For an SU(2) subgroup component of the SU(3) gauge group, it behaves like the SU(2) gauge field.

The relation between zero modes and the gauge field is relevant for the topological structure of QCD vacuum, e.g., the topological charge density distribution. It would be instructive to perform the similar analysis for topological properties with the overlap operator.

ACKNOWLEDGMENTS

The author is supported by a Grant-in-Aid for Scientific Research [(C) No. 20-363]. This work was supported by the Global COE Program, “The Next Generation of Physics, Spun from Universality and Emergence,” at Kyoto University. This work was in part based on the MILC collaboration’s public lattice gauge theory code (<http://physics.utah.edu/~detar/milc.html>). The lattice QCD simulations were carried out on Altix3700 BX2 and SX8 at YITP in Kyoto University.

[1] M. F. Atiyah and I. M. Singer, *Ann. Math.* **87**, 484 (1968).
 [2] T. Banks and A. Casher, *Nucl. Phys. B* **169**, 103 (1980).

[3] E. V. Shuryak and J. J. M. Verbaarschot, *Nucl. Phys. A* **560**, 306 (1993).
 [4] T. Guhr, A. Muller-Groeling, and H. A. Weidenmuller,

- Phys. Rept. **299**, 189 (1998).
- [5] J. J. M. Verbaarschot and T. Wettig, *Ann. Rev. Nucl. Part. Sci.* **50**, 343 (2000).
- [6] M. Göckeler, H. Hehl, P. E. L. Rakow, A. Schäfer, and T. Wettig, *Phys. Rev. D* **59**, 094503 (1999).
- [7] P. H. Damgaard, U. M. Heller, and A. Krasnitz, *Phys. Lett. B* **445**, 366 (1999).
- [8] P. H. Damgaard, U. M. Heller, R. Niclasen, and K. Rummukainen, *Phys. Rev. D* **61**, 014501 (1999).
- [9] S. Dürr, C. Hoelbling, and U. Wenger, *Phys. Rev. D* **70**, 094502 (2004).
- [10] E. Follana, A. Hart, and C. T. H. Davies (HPQCD Collaboration and UKQCD Collaboration), *Phys. Rev. Lett.* **93**, 241601 (2004).
- [11] K. Y. Wong and R. M. Woloshyn, *Phys. Rev. D* **71**, 094508 (2005).
- [12] E. Follana, A. Hart, C. T. H. Davies, and Q. Mason (HPQCD Collaboration and UKQCD Collaboration), *Phys. Rev. D* **72**, 054501 (2005).
- [13] M. Lüscher and P. Weisz, *Commun. Math. Phys.* **97**, 59 (1985); **98**, 433 (1985).
- [14] G. P. Lepage and P. B. Mackenzie, *Phys. Rev. D* **48**, 2250, (1993).
- [15] E. Follana, Q. Mason, C. T. H. Davies, K. Hornbostel, G. P. Lepage, and H. Trotter (HPQCD Collaboration), *Nucl. Phys. Proc. Suppl.* **129**, 447 (2004).
- [16] K. Orginos, D. Toussaint, and R. L. Sugar (MILC Collaboration), *Phys. Rev. D* **60**, 054503 (1999).
- [17] J. Smit and J. C. Vink, *Nucl. Phys. B* **298**, 557 (1988).
- [18] A. Yamamoto and H. Suganuma, *Phys. Rev. Lett.* **101**, 241601 (2008).
- [19] A. Yamamoto and H. Suganuma, *Phys. Rev. D* **79**, 054504 (2009).
- [20] A. Yamamoto, *Phys. Lett. B* **688**, 345 (2010).
- [21] H. Neuberger, *Phys. Lett. B* **417**, 141 (1998).
- [22] D. H. Adams, *Phys. Rev. Lett.* **104**, 141602 (2010).
- [23] P. J. Forrester, *Nucl. Phys. B* **402**, 709 (1993).
- [24] A. Yamamoto and H. Suganuma, *Phys. Rev. D* **81**, 014506 (2010).
- [25] J. J. M. Verbaarschot, *Phys. Rev. Lett.* **72**, 2531 (1994).
- [26] M. E. Berbenni-Bitsch, S. Meyer, A. Schäfer, J. J. M. Verbaarschot, and T. Wettig, *Phys. Rev. Lett.* **80**, 1146 (1998).